

Berkeley MRI Shimming Tool: Online B0 Shimming using Conformal and Local DC Arrays

Robert Peltekov



Electrical Engineering and Computer Sciences
University of California, Berkeley

Technical Report No. UCB/EECS-2024-163

<http://www2.eecs.berkeley.edu/Pubs/TechRpts/2024/EECS-2024-163.html>

August 9, 2024

Copyright © 2024, by the author(s).
All rights reserved.

Permission to make digital or hard copies of all or part of this work for personal or classroom use is granted without fee provided that copies are not made or distributed for profit or commercial advantage and that copies bear this notice and the full citation on the first page. To copy otherwise, to republish, to post on servers or to redistribute to lists, requires prior specific permission.

Acknowledgement

Thank you to Mikgroup for embracing and empowering me. To Miki: Thank you for the guidance and chance to be a part of such a great group of researchers. To Julian, Ekin, Shreya, Suma, Alfredo, and Rebekah: thank you for all that you showed me and the time you spent to make this project possible.

Thank you to Ana, Fred, Derek, Tarun for becoming such good friends and making this year worthwhile.

Thank you to Ava for the love and unwavering support <3.

Thank you to my family: Mimi, Mom, and Dad. I am blessed to be raised by you, brought to this world of opportunity, and to have your brightest thoughts and

intentions guide me
throughout life.

Berkeley MRI Shimming Tool: Online B_0 Shimming using Conformal and Local DC Arrays

by

Robert Peltekov

A thesis submitted in partial satisfaction of the
requirements for the degree of

Master of Science

in

Electrical Engineering and Computer Sciences

in the

Graduate Division

of the



University of California, Berkeley

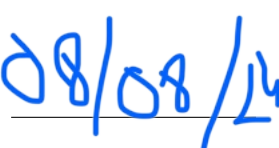
Committee in charge:

Professor Michael Lustig, Chair
Professor Chunlei Liu

Spring 2024

The thesis of Robert Peltekov, titled Berkeley MRI Shimming Tool: Online B_0 Shimming using Conformal and Local DC Arrays, is approved:

Chair **Michael Lustig** 


Date 
Date 08/08/2024
Date _____

Berkeley MRI Shimming Tool: Online B_0 Shimming using Conformal and Local DC Arrays

Copyright 2024
by
Robert Peltekov

Abstract

Berkeley MRI Shimming Tool: Online B_0 Shimming using Conformal and Local DC Arrays

by

Robert Peltekov

Master of Science in Electrical Engineering and Computer Sciences

University of California, Berkeley

Professor Michael Lustig, Chair

Developed to enhance MRI scan quality, the Shim Tool is a novel and adaptable software to correct B_0 field inhomogeneity using local and conformal DC coil arrays. The Shim Tool orchestrates this operation by automating actions between an MRI scanner in sync with commanding currents in shim loop elements powered by the Open Source Current Driver. A custom-built array of shim coils, designed to be conformal and malleable, were used by the Shim Tool to reduce improve B_0 field inhomogeneity. Root mean squared error (RMSE) of the fieldmaps was reduced by 63 percent on average and improved bSSFP/EPI image quality across 2D scans of a spherical ball phantom. The tool and developed hardware provide a means to shim any FOV using low-profile hardware in multi-modal studies, such as TMS/EEG/fMRI, and generally improve the acquisition quality of any MRI machine.

To Mimi, Mom, and Dad.

Contents

Contents	ii
List of Figures	iv
1 Introduction	1
1.1 Motivation	1
1.2 Project Goals	2
1.3 Relevant Work	3
2 Background	4
2.1 Magnetism	4
2.2 MRI Concepts	5
Spins and the MR Signal	5
Gradients	6
Magnetic Susceptibility	8
Linear and Higher Order Shims	9
Basic Pulse Sequence Terminology and Characteristics	9
Fieldmaps	10
3 Methodology	11
3.1 Setup Details	11
3.2 Current Driver and Scanner API	12
Current Driver System	12
Scanner Automation: ExSI	13
3.3 Shim Procedure	13
3.4 Simulations	14
4 Design	17
4.1 Local Shim Array	17
4.2 Tool System Design	20
Scanner Control	20
Shim Control	21

Interface	22
Use Case and Optimizations	22
5 Experimentation and Results	25
6 Discussion	32
6.1 Conclusion	32
6.2 Future Work	32
AC/DC Coil Integration	32
Shim Tool Feature Improvement	33
Bibliography	34
A Code	36

List of Figures

- 2.1 Depiction of a loop of radius R with current amplitude I flowing through it. The direction of B in the center of the loop is normal to the plane of the loop. 4
- 2.2 Reproduced from Nishimura. The depicted proton spins, once aligned in a unidirectional magnetic field \vec{B}_0 . The total magnetization \vec{M}_0 is the sum of magnetizations from every location $\vec{M}_0(x, y, z)$ within the relevant volume. 5
- 2.3 Reproduced from Nishimura. **Left:** the spin's moment begins precession. **Middle:** as \vec{B}_0 is exposed for a sufficient amount of time, the spin will rotate or "tip" into the transverse plane. **Right:** the trajectory of a spin in the rotating frame excited by a 90 degree excitation pulse. 6
- 2.4 Reproduced from Nishimura. A square water object given only \vec{B}_0 in the left and \vec{B}_0 plus some gradient \vec{G}_x on the right. As can be seen in **(a)**, the signal emitted from the object fully lies at one frequency with a small bandwidth because the entire volume can be characterized with a constant B_z strength equal to B_0 . In **(b)**, the bandwidth widens because the linear gradient, G_x , varies B_z with respect to the actual position. This means that a water in the box at a larger x offset will emit MR signal at a slightly higher frequency than Larmor frequency. 7
- 2.5 Reproduced from Schenck. Magnetic susceptibility from a sphere and cylinder in B_0 field. The top panel depicts the shape and orientation, and the bottom shows the change in magnetic field strength over space. 8
- 3.1 The GE Discovery MR750W 3.0T Scanner is used in this project. Installed is the GE Head Coil that is used for transmit and receive signal throughout this project on the small spherical phantom. The scanner features a 3 Tesla B_0 magnet, with linear gradients for shimming and scanning, all housed within the bore of the machine (the donut-looking section of the machine). There are no higher order shims included with this scanner. The \vec{B}_0 is depicted and is aligned with the z direction of the scanner. The effective \vec{B}_1 field is in the transverse (x - y) plane. 11
- 3.2 Reproduced from Veys[21] and Calleja[4].The boards that comprise the current driver system. From left to right: current driver board, fiber optic relay, Teensy microcontroller board[2]. 12

- 3.3 The process of shimming, reproduced from Maravilla[11]. Using an initial B_0 map and basis maps from each individual coil, currents, x , are computed for which to apply. An effective B_0 field is then composed from the summation of each shim coil field given their prescribed currents. That is then in an ideal case added to the initial B_0 field to achieve net zero off resonance. 13
- 3.4 From left to right: the idealized headcap of 15 integrated Rx and Shim coils for use in the TMS-EEG-fMRI research work, reproduced from Maravilla[11]. The ball phantom used to generate background field map. The simulated ball phantom with an array of 15 coils placed around it in the same configuration as the the Rx Headcap. 15
- 3.5 Simulation results from shimming off resonance caused by a TMS coil in the three configurations. Provided is a B_0 mapped slice of the original phantom with induced off resonance due to the TMS Coil, and then the simulated expected shimming performance capable with the 15 channel Head Array depicted above. The standard deviation is provided both per both highlighted slice and for the total volume shimmed per slice. 16
- 4.1 AC/DC Circuit. **Left** shows the circuit diagram of a typical RF receive coil. It features DC feed points which block the Larmor Frequency and AC feed points with DC blocks via capacitors. **Right:** initial PCB layout to allow for shim components on one side and RF components on the other. 17
- 4.2 The blocking circuits implemented and tuned on one of the physical PCBs, showing sufficient impedance and blocking close to the Larmor Frequency. 18
- 4.3 Tuning Process for proton traps. **a)** Shows the blocking LC circuit soldered onto a smaller V2 board. A 33 pF capacitor and a 47 nH inductor are used for the circuit. The inductor is then widened to increase the resonant frequency until the VNA display (seen in Figure 4.2) shows resonance at the Larmor Frequency, 127.7 MHz. **b)** Because the inductor is still malleable after tuning and handling it will likely de-tune the trap, it is covered in hot glue to hold its position. . . . 19
- 4.4 8 shim loops constructed, each with its own lead going to the shim current driver. In V1, Caterpillar Traps are featured wrapping the wire to induce blocking of common mode currents along the leads themselves[9]. In V2, the boards containing the proton traps were minimized to reduce B1 artifacts caused by the wire traces on the boards. In V3, an extra blocking proton trap was added in-line to each of the shim loops to further reduce Larmor Frequency. V2 and V3 also feature individual baylun traps instead of the catarpillar traps. 19

4.5	System Overview of the Shim Tool. The tool itself runs on a separate computer from the MRI Console for software availability and different scanner version compatibility. It features two client services that control direct connectivity with the ExSI Server on the MRI Console and the boards controlling the actual shim array in the scanner. The Shim tool synchronizes asynchronous operations between ExSI and the Shim Drivers, provides a user interface that describes current operations, and allows a user to begin a host of optimally shimmed scans with a defined ROI at their will.	20
4.6	The Introductory view of the Shim Tool. Shows a log of ExSI Client-Server interaction, and allows the user to queue up predefined scan operations in addition to viewing axial slices one by one on the left. In addition to viewing the latest scan magnitude data, this view also allows the user to load the original magnitude image of the obtained background and define an ROI by overlaying an ellipsoid in transparent red. This ROI effectively truncates the data that is used to form basis vectors and the original background field. It is re-definable however many times the user wishes.	23
4.7	The Shim View of the Shim Tool. Shows log of communication with the Shim Drivers. It allows you to manually set currents to the shim loops, control the currently viewed slice index, set the delta TE between scans of phase images, obtain background or shimmed fieldmaps, loop and gradient basis maps. The left panes allow the user to switch between viewing the selected slice for either the background, the expected potential shim result, and the actual shim result of the scanned object. The bottom left allows the user to see statistics on each image and also save both data and statistics of performance of the shims once they have been acquired.	24
5.1	Setup of Phantom and shim loops. a) The sphere phantom with 8 shim loops taped around the phantom. They are arranged with one loop in an axial position in the center and 7 loops around it. b) The same sphere phantom is covered by a 3mm thick head mask with shim elements taped around it in the same orientation as in (a). A head mask with stitched on AC/DC elements will eventually facilitate a simple method for equipping the coils to the subject.	26
5.2	Experimental setups to induce off-resonance. a) The shim-loop-equipped phantom with two water bottles to induce B_0 off-resonance. b) With one water bottle. c) With a TMS Coil. The off-resonance from a TMS Coil, and the robot arm around it, is largely the motivation for this project.	27

5.3	Shim performance, as observed by the Shimming Tool, in terms of visualized B_0 maps for each experiment. The Background, Expected, and Achieved B_0 fieldmaps are shown for all three experiments. The Background is the fieldmap without any shimming done. The Expected is the fieldmap that the shim tool computes that it should achieve. The Achieved is the fieldmap observed after shimming. Note: the color scales of the 2 Bottle and 1 Bottle experiments are on the order of 300 Hz, while the TMS coil experiment is on the order of 40 Hz. The standard deviation and mean of off-resonance in the slice is shown in terms of Hz for each fieldmap. The Shim Tool and hardware reduce overall root mean squared error by 63 percent on average.	28
5.4	Histogram showing voxels binned by the amount of off-resonance they have for each experiment. In each histogram, the Background, Expected, and Shimmed corrected fieldmaps are shown in different colors. The Background is the fieldmap without any shimming done. The Expected is the fieldmap that the shim tool computes that it should achieve. The Shimmed is the fieldmap observed after shimming.	29
5.5	2 Bottle Experiment: bSSFP images before and after shimming. They were acquired with a 24 by 24 cm FOV in the same position that the shim tool was correcting and 256 frequency and phase encodes. The bSSFP scan has a TE of 2.3 ms and TR of 6.7 ms	30
5.6	1 Bottle Experiment: bSSFP and single shot EPI images before and after shimming. They were acquired in the same position that the shim tool was correcting. The bSSFP scan has a TE of 2.1 ms, TR of 6.3 ms, 24 by 24 cm FOV, with 224 frequency and phase encodes. The EPI scan has a TE of 20.1 ms and TR of 149 ms, 22 by 22 cm FOV, with 96 frequency and phase encodes.	31

Acknowledgments

I would like to sincerely thank Miki Lustig for the support and insights that he continually gave me throughout the project. You graciously let me be a part of your research group and gave me the privilege to use such invaluable equipment and learn from such amazing students / role models. I was so warmly embraced in this new family and am so lucky to have had the chance to grow around everyone in the group.

Thank you to Julian Maravilla for the direct mentorship and hands on help with this project. I am so grateful for the countless hours you spent teaching me concepts I wasn't familiar with, showing me the ropes to making new hardware (as well as training me on all the equipment I needed to use), and troubleshooting with me when things inevitably didn't work. I would have been lost in this project without your efforts and would not have been able to get this far. Thank you to Ekin Karasan, Shreya Ramachandran, Suma Anand, and Alfredo De Goyeneche for your time, continual advice, and guidance throughout the last two and a half years. You were all always ready to make time for my many questions, give tips/tricks to present my data, help learn new software, and share advice for every situation or predicament I was in. And a sincere thank you to Rebekah Zhao for introducing me to the group and being my first research mentor. I learned so much working under you for the MRDust project and am so grateful for the support you have always provided while I've been a part of the group.

Thank you to Jason Stockmann for your dedicated input and expert perspective regarding shimming and helping me build better hardware.

Thank you to Ana Cismaru and Frederic Wang for being my M.S. buddies to lean on within MikGroup for the year. Thank you to my roommates Tarun Amarnath and Derek Yao for becoming the closest friends I had at Berkeley this year and filling my extra time with joy and excitement.

Thank you to Ava for the love and support that you surrounded me with as I pursued this work, and for always believing in and empowering me.

Lastly to my family: Mom, Dad, and Mimi, thank you for lighting my path with love and care and opening every door along my path. I am blessed to be raised by you, brought to this world of opportunity, and to have your brightest thoughts and intentions guide me throughout life.

Chapter 1

Introduction

1.1 Motivation

Magnetic Resonance Imaging (MRI) is a sophisticated and customizable modality widely known for its ubiquity and unparalleled capabilities in imaging soft tissue in the human body. MRI's capacity to image arises from its application of Radio Frequency (RF) pulses and magnetic fields in conjunction to “excite” a response—the Magnetic Resonance (MR) signal—from the subject. The MR signal reflects unique physical properties of the subject. This modality is derived from the phenomenon of Nuclear Magnetic Resonance (NMR), which describes the natural magnetic moments (spins) of atomic nuclei with odd number protons and neutrons in any substance. As such, MRI could be used as a tool in many fields, such as organic chemistry and material science, in addition to the presumed medical/biology space.

There is a direct correlation between the frequency of the excited MR signal the strength of the main magnetic field (B_0). MRI scanners aim to maintain constant B_0 field across the imaging volume because imperfections in this main field negatively affect the acquisition and reconstruction of the MR signal. Specifically, field inhomogeneity directly results in artifacts such as signal loss, distortion, and inaccurate spatial representation in the resultant images, which can severely limit the diagnostic utility of MRI[19]. Refer to Chapter 2 for a more detailed description of the NMR phenomenon and how B_0 field homogeneity impacts image quality. In essence, these imperfections naturally motivate the need to “shim,” or correct, the imperfections of the B_0 field within the region of interest (ROI).

All objects exposed to an external magnetic field alter that field due to susceptibility-induced magnetization. In the context of MRI, this manifests as unwanted fluctuations in the main B_0 field. In humans, field inhomogeneity typically arises at the interfaces between tissues of different magnetic susceptibilities (e.g., air and soft tissue) or within regions with complex anatomical structures. These imperfections are amplified and even more critical to counteract in scanners at ultra high field (UHF) strengths where smaller details are sought to be imaged.

Shimming mitigates these inhomogeneities through both passive and active methods. Passive shimming is static and typically set during the installation of the MRI scanner. In contrast, active shimming adjusts the magnetic field to adapt to specific imaging scenarios or patient profiles. This is done through the use of shim coils or loops that generate magnetic fields to counteract the observed inhomogeneities via direct current in their filaments. Active shims can be broadly categorized into first-order (linear) and higher-order shims. First-order shims are already a part of most scanners due to the preexisting need for gradient coils. Higher-order shims might be incorporated as an extension of the scanner’s existing hardware, or via multi-coil (MC) arrays that are externally added. MC arrays provide highly localized shimming capabilities with smaller required currents due to their proximity. This project focuses on the implementation of new conformal and local MC shim arrays.

1.2 Project Goals

There has been a concerted effort among research groups to develop closed-loop multi-modal investigation techniques, such as TMS/EEG/fMRI, to obtain deeper insights into brain function[15][16]. These techniques are specifically hindered by B_0 susceptibility artifacts caused by required hardware, like an EEG head cap and the TMS coil itself, in the bore. While passive shimming techniques have been shown to reduce artifacts, they are dependent on the orientation of the TMS coil[3]. Dynamic shimming techniques would allow for intra-scan repositioning of the TMS coil. The GE MR750 3T scanner used in this project only features first-order dynamic shims, and there is need for more accurate local shims. More notably, there are significant space limitations in multi-modal studies namely due to the presence of various hardware in the bore. The integration of shim functionality within elements of a low profile receive array, such as the RF-EEG[12] or the 15 Channel Twisted-Pair Cap[11], is highly desired. Additionally, several other MRI-oriented research projects would benefit from being able to scan both phantoms and subjects with much more homogeneous B_0 fields.

In practice, there are a host of methods to dynamically and locally shim a desired ROI. Many 3rd party tools might interface with available shimming hardware[2]; however, they perform shimming offline and provide little interoperability with the scanner used in this project. “Online” refers to the process of computing and applying solutions in an integrated process with the scanner, allowing continuous scanning without interruptions, as opposed to “offline” solutions. The goal of this thesis work is to develop software and hardware for a highly configurable, local/conformal shimming solution and integrate it with an MRI scanner. This tool would enable higher image quality and design flexibility for a variety of imaging experiments conducted on the GE scanner. Namely, it would consist of the following capabilities:

- Function with a configurable number of shim elements.

- Obtain basis functions characterizing B_0 fields each element can generate in a quick “calibration sequence.”
- Compute optimum solutions for shimming any slice or ROI of the field of view (FOV) online.
- Integrate with the scanner and dynamically apply shim currents in sync with scan.

1.3 Relevant Work

In 2021, Celine Veys and Rafael Calleja integrated the same shimming current drivers used in this project with the Aspect Wrist II 1T MRI System and showed a variety of coil configurations improving image quality without degrading the transmit field and receive SNR[21][4]. Their work serves as an additional proof of concept and validation for using the Open Source Shimming current drivers in MRI systems.

There are publications of “AC/DC” Coil Arrays[20] and a number of papers about the Integrated Parallel Receive, Excitation, and Shimming (iPres) array[5], showing that sufficient shim performance in clinical scanners at 3 Tesla could be achieved with modest currents of 1-2A in local MC arrays with single turn loops. Jason Stockmann et al. have developed several iterations of “AC/DC” B_0 shim and RF receive arrays for 7T with implementations of 31-channel systems and designs for up to 64-channel fixed local arrays[19].

The Shimming Toolbox[2] is an open source framework that enables shimming control of the Open Source Shim Drivers used in this project with APIs to interact with Siemens Scanners. It is used mainly for offline shim reconstruction and provides little tuneability for other systems. Jordan Grelling proved the usability and efficiency of GE’s scanner automation tool, ExSI, which is extensively used within this work[7].

Chapter 2

Background

This section provides an overview of the required knowledge to understand fundamentals of image formation in MRI and why shimming is necessary in modern MRI systems.

2.1 Magnetism

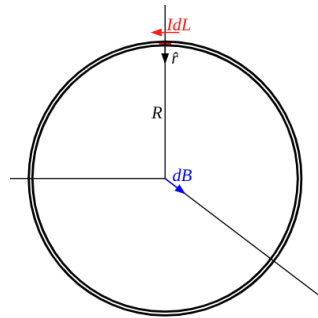


Figure 2.1: Depiction of a loop of radius R with current amplitude I flowing through it. The direction of B in the center of the loop is normal to the plane of the loop.

The Biot-Savart Law[6] can be used to compute the magnetic field, \vec{B} , at a specific point, \vec{p} , generated by current, I , flowing along a path, C :

$$\vec{B}(\vec{p}) = \frac{\mu_0 I}{4\pi} \int_C \frac{\partial \vec{l} \times (\hat{r})}{\|\vec{r}\|^2} \quad (2.1)$$

where μ_0 represents the magnetic vacuum permeability constant, $\partial \vec{l}$ is the infinitesimally small vector of the direction of current in path C , \vec{r} is the vector from \vec{p} to $\partial \vec{l}$, and \hat{r} is the unit vector in same direction as \vec{r} . Solved for the point directly in the center of a single turn

circular loop as shown in Figure 2.1, the equation becomes:

$$\vec{B} = \frac{\mu_0 I}{2R} \quad (2.2)$$

where R is the radius of the loop. This simplification is of notable interest because this project deals with approximately circular single turn loops and this is an easy way to check validity of field strength from one loop in obtained B_0 maps.

It is convenient to think a magnetic field as the sum of several orthogonal fields[10]. This concept of adding and subtracting field components is how shimming—crafting a more homogeneous B_0 field—is achieved.

2.2 MRI Concepts

The content here is largely inspired by Nishimura’s Principles of Magnetic Resonance Imaging[13], and Michael Lustig’s spring 2023 introductory MRI course, EE225e, at UC Berkeley.

Spins and the MR Signal

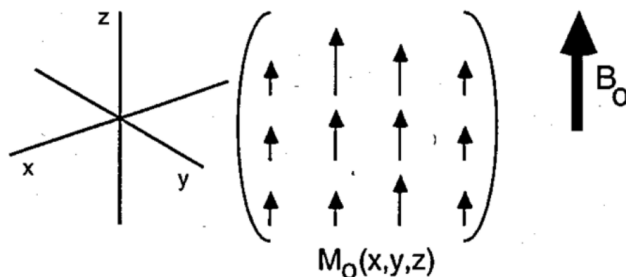


Figure 2.2: Reproduced from Nishimura. The depicted proton spins, once aligned in a unidirectional magnetic field \vec{B}_0 . The total magnetization \vec{M}_0 is the sum of magnetizations from every location $\vec{M}_0(x, y, z)$ within the relevant volume.

The NMR phenomenon arises due to the fact that nuclei with an odd number of protons and/or neutrons have an inherent angular momentum or a nuclear spin. Hydrogen, ^1H , is conveniently the most abundant atom in the human body that exhibits this phenomenon. As a result, it is the most commonly targeted nucleus in MRI. Absent some external magnetic field, the net sum of all nucleic moments in the field of view is effectively zero because they are randomly oriented. Under the influence of a strong magnetic field, referred to as B_0 , the spins align their moments with the direction of \vec{B}_0 as shown in Figure 2.2. In clinical scanners, the strength of the B_0 field is usually 3 Tesla (T), but ranges from 0.5 to 7 Tesla.

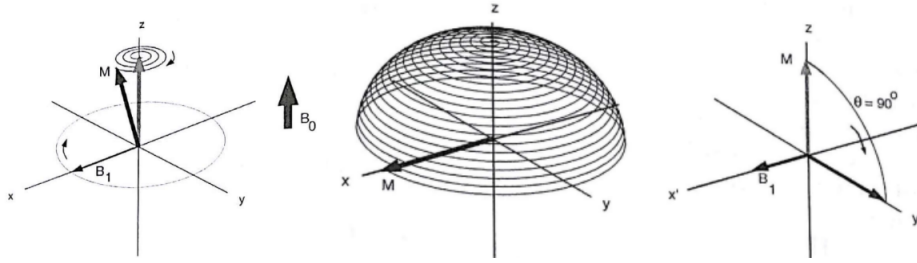


Figure 2.3: Reproduced from Nishimura. **Left:** the spin's moment begins precession. **Middle:** as \vec{B}_0 is exposed for a sufficient amount of time, the spin will rotate or "tip" into the transverse plane. **Right:** the trajectory of a spin in the rotating frame excited by a 90 degree excitation pulse.

The unified alignment of magnetization, \vec{M}_0 , is the net sum of every exposed proton and is proportional to strength of B_0 .

By convention, the direction of \vec{B}_0 is defined as the \hat{z} direction in the scanner. Notably, the frequency at which these spins rotate is directly proportional to the strength of the magnetic field that they are in as well. This frequency is known as the Larmor frequency (127.7MHz at 3.0T), and it is governed by the equations:

$$\omega = \gamma B \quad (2.3)$$

$$f = \frac{\gamma}{2\pi} B \quad (2.4)$$

in which ω is the atom-specific gyromagnetic ratio. For the Hydrogen proton, $\frac{\gamma}{2\pi} = 42.587$ MHz/T. The MR signal from these proton spins is produced in the following manner: while exposed to a static \vec{B}_0 , an RF pulse (a time-varying magnetic field, \vec{B}_1) at the Larmor frequency is applied and exposed protons absorb it beginning a process known as "excitation." This excitation manifests as the magnetization of the spins "tips," or more formally torques and precesses, out of the equilibrium state into the transverse plane as Figure 2.3 describes.

The spins or magnetic moments, now rotating in the transverse plane, emit the time-varying magnetic field known as the MR signal, which will induce a detectable voltage in a receiving coil tuned to the same Larmor frequency. Individually, the signal produced by a single proton is minuscule, but in undisturbed unison the total signal produced by all excited spins in the scanner is significant enough to read out. Over time, the magnetization in the transverse plane decays and independently the longitudinal (in the direction of \vec{B}_0) magnetization recovers in a process called relaxation.

Gradients

Recall that the gyromagnetic ratio of a nucleus is the precise relationship between the strength of \vec{B}_0 and the frequency at which its magnetic moment will spin at. Thus, all spins

of one nucleic species within the imaging volume will produce signal at the same frequency. However, if different regions experience different B_0 strengths, then their corresponding nuclei will resonate at their own Larmor Frequencies. This concept is leveraged in MRI by using gradient fields which superimpose a linear spatially varying magnetic field on top of B_0 . These gradient fields ultimately create a mapping between physical space to the frequency at which nuclei will resonate. Figure 2.4 illustrates this critical concept.

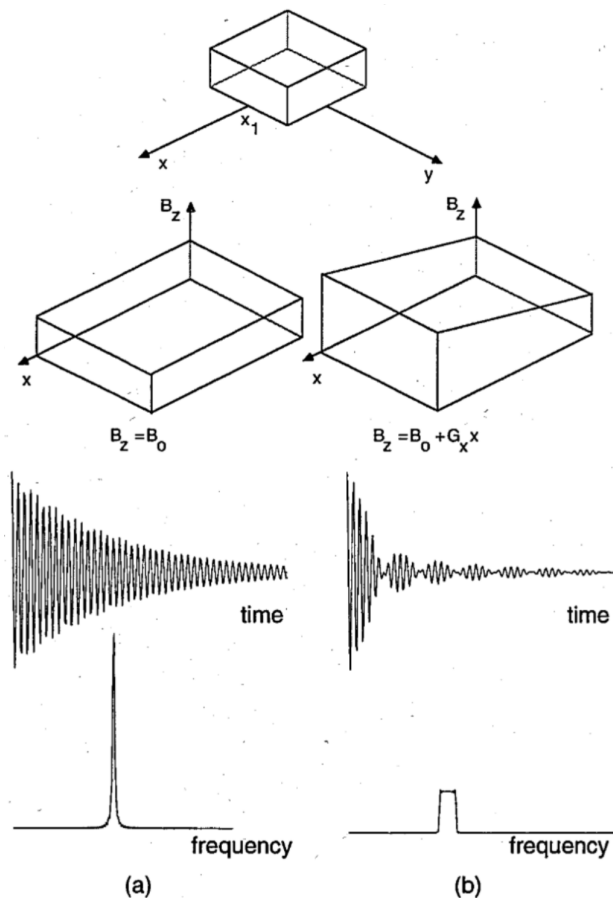


Figure 2.4: Reproduced from Nishimura. A square water object given only \vec{B}_0 in the left and \vec{B}_0 plus some gradient \vec{G}_x on the right. As can be seen in (a), the signal emitted from the object fully lies at one frequency with a small bandwidth because the entire volume can be characterized with a constant B_z strength equal to B_0 . In (b), the bandwidth widens because the linear gradient, G_x , varies B_z with respect to the actual position. This means that a water in the box at a larger x offset will emit MR signal at a slightly higher frequency than Larmor frequency.

By varying linear gradients in all three dimensions, \vec{G}_x , \vec{G}_y , \vec{G}_z , over the course of an acquisition, the received frequency domain signal could be reconstructed into an image do-

main signal using the Fourier Transform. The specifics of how images are acquired with specific contrasts in MRI systems using these linear gradient mappings will not be covered, and the reader is referred to Nishimura[13] to glean more upon their discretion. It suffices to say that whenever there are discrepancies in the magnetic field, diverging from the ideal \vec{B}_0 or purposefully applied gradient fields, the resulting reconstructed image loses information where that proper “mapping” is degraded.

Magnetic Susceptibility

It would be convenient if the main \vec{B}_0 remains constant and unchanged from its calibration during magnet installation and when it is used to scan some object. This is unfortunately impossible because any foreign object placed in an external magnetic field induces distortions from the original field[17]. It is quite difficult to estimate this effect as it requires exact computation and summing of total field perturbations, and the immense number of subtle varieties in objects that enter the scanner is too great. Figure 2.5 depicts how for simple spherical and cylindrical objects the static magnetic field is distorted around and within their volumes. Notice how at the boundary of different mediums there are significant space varying distortions. These kinds of distortions are often observed in scans of the human body near many varying air/tissue boundaries. Examples include the artifacts near the sinuses when attempting to image the head or brain and near the lungs when attempting to image the abdomen or heart.

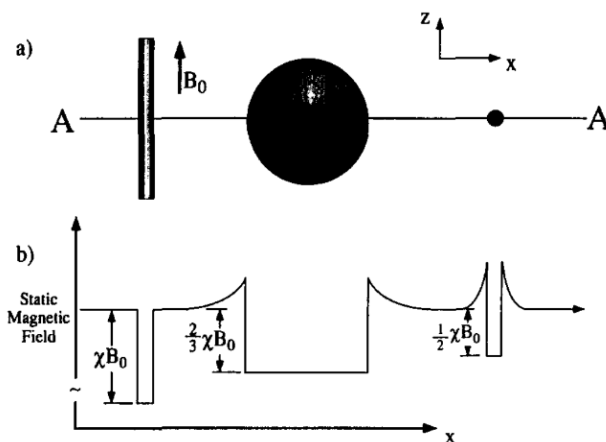


Figure 2.5: Reproduced from Schenck. Magnetic susceptibility from a sphere and cylinder in B_0 field. The top panel depicts the shape and orientation, and the bottom shows the change in magnetic field strength over space.

Linear and Higher Order Shims

The hardware which create gradient fields for obtaining images is what initially provides MRI scanners ability to attempt correcting or “shimming” inhomogeneity in the main magnetic field. In addition to linear gradients, scanners may include more complex embedded coils that approximate higher order spatial varying fields, \vec{B}_z . For example, Spherical Harmonic Shims could compose second or third order field variations. At their core, these gradient and shim coils are just windings with direct current flowing through them. Since gradients must be housed within the bore of the MRI scanner, a significant distance from the region of interest, they require large currents to desirably shim due to the $||\vec{r}'||^2$ term in the Biot-Savart equation. For reference, to achieve the 30 to 50 milliTesla per meter (mT/m) field strength that gradient coils typically need to output, they require currents in the range of 100 amps to over 500 amps. This high current requirement and limited high order function approximation motivates the specific use case of small local shim coils close to the region of interest. It has been shown that local shim coils can achieve similar field strengths with 1-2 amps delivered to independent loops[19].

Basic Pulse Sequence Terminology and Characteristics

The RF pulse, the three linear gradients, and the receiver coil are used in a specific interleaved manner, called a pulse sequence, to both manipulate the magnetization, \vec{M} , and extract a meaningful MR signal from within the scanner. Different pulse sequences might include any number of composed gradient waveforms, RF excitation pulses, and timing to collect data. Individual pulse sequences are themselves further categorized by the following fundamental parameters that define the shape of the sequence. Notable parameters include but are not limited to:

- Center Frequency (CF): While not specifically a protocol parameter, this dictates the exact center strength of the B_0 field.
- Time to Echo (TE): The time between excitation and signal readout.
- Repetition Time (TR): The time between successive excitation.
- Field-of-View (FOV): The physical dimensions of the acquired image. Determined by frequency of sampling.
- Resolution: The physical resolution of the acquired image. Determined by coverage of K-Space.

Resolution and field of view together could be used to compute the size of a voxel within an image. The resulting intensity of a voxel is the summation of signal from every spin residing in the volume of that voxel.

Fieldmaps

Since signal is acquired over a period of time during which spins precess, it accrues phase. Different spins exposed to different field strengths, by lieu of gradients or field imperfections will precess at different rates and cause phase differences across the images. At the microscopic level, phase differences (referred to as dephasing) of spins residing within a single voxel cause signal cancellation and result in lower signal intensity measured from that position. At the macroscopic level, phase differences between voxels will correlate the field strengths between those positions in space. This idea is formalized into a method to map field strength in the FOV from images acquired using the following equation[14]:

$$\frac{\angle(I_{TE_1}^* \cdot I_{TE_2})}{\Delta TE} \quad (2.5)$$

Taking two scans with different TE and all other scan parameters the same will simply result in two different samplings of phase accrual from the precession of the signal. For two images, TE_1 and TE_2 , a fieldmap of the FOV could be extracted using Equation 2.5. This equation takes the phase difference of two images, $\angle(I_{TE_1}^* \cdot I_{TE_2})$ which I will call the difference phase image, and uses the difference in their snapshot times (TE) to convert the phase difference into relative field strengths. The field offset at a position is typically denoted in terms of Hz due the direct conversion one can make using the gyromagnetic ratio, γ .

Given that the difference phase image has a range of $-\pi$ to π , there is an implicit limit of $\pm \frac{1}{2\Delta TE}$ Hz that a fieldmap can naturally describe. Decreasing TE might increase the range of offresonance viewable without any phase wraps, but it will also increase the noise in the measurement. As such, a phase unwrapping algorithm and procedure is generally necessary to improve the robustness of measurements and accuracy of B_0 field maps[8].

Chapter 3

Methodology

3.1 Setup Details

This project is part of an effort to build closed-loop testing infrastructure for TMS-EEG-fMRI brain studies. There will be significant hardware in the bore, and the space that remains for shimming between the head and the variably positioned TMS coil is quite limited. As such, the developed loops must eventually be integrated into the Rx Coils as AC/DC loops. The scanner used is shown in Figure 3.1.



Figure 3.1: The GE Discovery MR750W 3.0T Scanner is used in this project. Installed is the GE Head Coil that is used for transmit and receive signal throughout this project on the small spherical phantom. The scanner features a 3 Tesla B_0 magnet, with linear gradients for shimming and scanning, all housed within the bore of the machine (the donut-looking section of the machine). There are no higher order shims included with this scanner. The \vec{B}_0 is depicted and is aligned with the z direction of the scanner. The effective \vec{B}_1 field is in the transverse (x - y) plane.

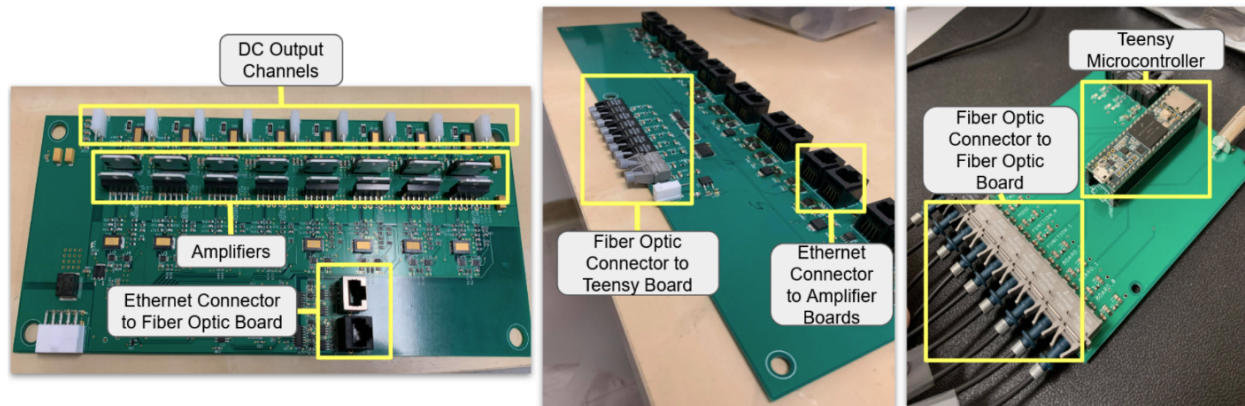


Figure 3.2: Reproduced from Veys[21] and Calleja[4]. The boards that comprise the current driver system. From left to right: current driver board, fiber optic relay, Teensy microcontroller board[2].

3.2 Current Driver and Scanner API

Current Driver System

A team at Massachusetts General Hospital has generously gifted the Opensource Imaging Current Driver system[2] shown in Figure 3.2. This system consisted of three components:

- Teensy Arduino Microcontroller with Motherboard
- Fiber Optic Relay Board
- Current Driver Board(s)

The Teensy Arduino controller receives commands over USB and relays them to the current driver hardware. Commands include calibrating the op amps on the current driver board, setting specific shim currents, or reading out active currents for specific channels. The Fiber Optic Relay Board is the relay and multiplexer between the microcontroller and up to 8 current driving boards. This board is connected to the Teensy via fiber cables so that it could easily communicate over the large distance from the console room to scanner room without any interference to / from the scanner. The Current Driver Boards are switching current sources that can individually supply 8 channels (shim loops), with up to 8A of controlled DC current each. They are fast-control-loop current source drivers so that they can compensate for the induced currents caused by the constantly changing gradient fields. This current driving system was largely assembled by Veys and Calleja during their respective Masters theses[21][4]. Their setup and efforts proved how the system would be useful for the current project today.

Scanner Automation: ExSI

An MRI scanner is typically operated by selecting protocol suites with multiple sequences, adjusting each of their parameters through the user interface and manually exporting any desired acquisition data off afterwards. This is typically a pretty long process on the order of tens of minutes. Scanners might also offer an API layer for automation. In the case of the GE MR750 scanner, it is called ExSI. This service runs on the scanner machine, and allows another host to connect via tcp socket, and send commands for the scanner to execute. Jordan Grelling conducted his Masters thesis work around creating a proof of concept implementation of an ExSI user client and automating tasks for the Beat Pilot Tone project[7][1].

3.3 Shim Procedure

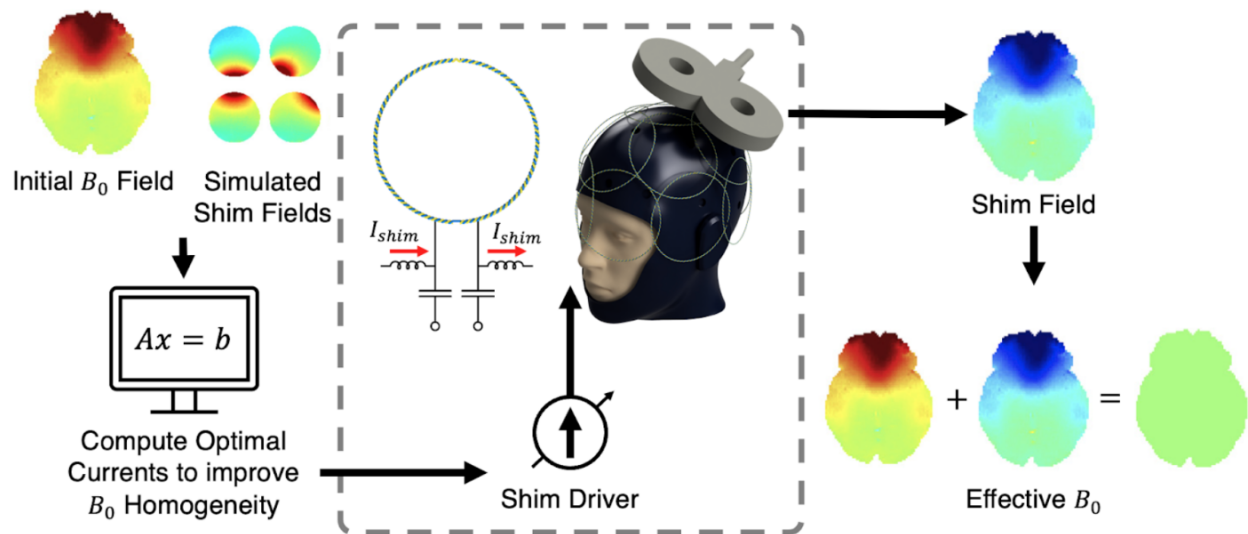


Figure 3.3: The process of shimming, reproduced from Maravilla[11]. Using an initial B_0 map and basis maps from each individual coil, currents, x , are computed for which to apply. An effective B_0 field is then composed from the summation of each shim coil field given their prescribed currents. That is then in an ideal case added to the initial B_0 field to achieve net zero off resonance.

Shimming is performed by first collecting a fieldmap of the background to characterize the inhomogeneity that is already present in the FOV. Throughout this study, a 20 cm diameter spherical ball phantom is used and fieldmaps are acquired using two 3D fast gradient echo sequences with altered TE's, as discussed in Section 2.2. First, a background fieldmap is obtained for the desired FOV after a prescan has been performed and all the shim loops are

at 0 amps. A fieldmap is then acquired for every loop in the array at 1 amp independently. Subtracting out the background fieldmap from each of the raw 1A loop fieldmaps results in the "basis" map for each respective loop. A basis fieldmap acts as a function, or effectively a vector basis, that defines the solution space reachable by a specific coil because field strength is linearly proportional to the current flowing through it. After basis functions are taken, the intersection of their signal-producing voxels and the user-defined ROI is used as a mask with which to vectorize the basis fieldmaps that makeup the columns in matrix A . The same mask is applied to the background fieldmap to create initial offset vector b .

Least squares is applied to solve for the exact currents that each loop should output, x , to cancel out deviation in b :

$$\begin{aligned} \min_x \quad & \|Ax + b\|_2 \\ \text{s.t.} \quad & \|x\|_\infty < 2 \end{aligned} \tag{3.1}$$

There is an imposed limit, $\|x\|_\infty < 2$, because the current to any loop should not exceed 2 amps as required by the Open Source Current Drivers. The basis map of the loops could also be acquired using the difference of a loop at 0.5 amps and -0.5 amps, effectively subtracting out the background and also averaging two measurements of output from the shim driver. A quick, but more noisy way, to address phase wrapping in the basis fieldmaps is to simply use a smaller current than 1A, and then scale up the obtained fieldmap by the same factor. Equation-3.1 is only useful if one wanted to compute the shim currents for reducing offresonance over the whole image volume. In practice, most MRI scans of a volume are done by stacking several 2D slices, thus it makes more sense to optimize for the specific slice that the scanner is imaging:

$$\begin{aligned} \min_x \quad & \|A_i x + b_i\|_2 + \psi \|(A_{i-1} + A_{i+1})x + b_{i-1} + b_{i+1}\|_2 \\ \text{s.t.} \quad & \|x\|_\infty < 2 \end{aligned} \tag{3.2}$$

Currents, x , for slice i are optimized in consideration of the effect the shims will have on neighboring slices $i \pm 1$ to ensure both that the fieldmap gradient is smooth across slices and that applied shim currents do not cause too much dephasing within a single voxel. ψ is a hyperparameter used to scale the optimization with respect to the neighboring slices.

3.4 Simulations

While the ultimate goal is to use the shim loops on a human head, a sphere phantom is used for approximation in this project. Because this project is geared towards reducing off resonance caused by hardware from the TMS-EEG-fMRI experiments, off resonance is induced by placing an actual TMS coil around the sphere phantom and using that as a background to correct. The position of each shim loop is generated in software and the basis map for each is computed using the Biot-Savart law for all voxels in the region of interest. Figure 3.4 shows the simulation objective, the ball phantom, and the simulated ball phantom with shim loops arranged around it. Figure 3.5 shows the results of this simulation.



Figure 3.4: From left to right: the idealized headcap of 15 integrated Rx and Shim coils for use in the TMS-EEG-fMRI research work, reproduced from Maravilla[11]. The ball phantom used to generate background field map. The simulated ball phantom with an array of 15 coils placed around it in the same configuration as the the Rx Headcap.

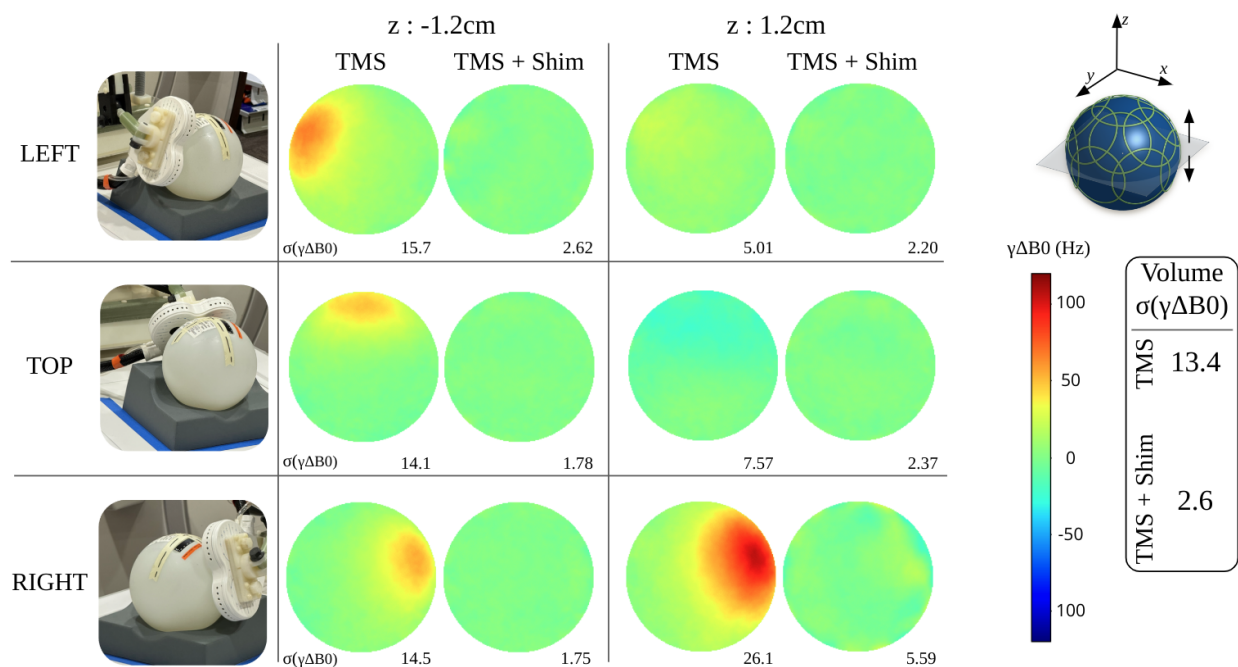


Figure 3.5: Simulation results from shimming off resonance caused by a TMS coil in the three configurations. Provided is a B_0 mapped slice of the original phantom with induced off resonance due to the TMS Coil, and then the simulated expected shimming performance capable with the 15 channel Head Array depicted above. The standard deviation is provided both per both highlighted slice and for the total volume shimmed per slice.

Chapter 4

Design

4.1 Local Shim Array

The shim loops are predominantly 10cm in diameter, although this value is modifiable depending on the size of the RF coils that are ultimately desired. The current sources are limited to 2A of current in either direction. The loops will be conformal and simply attached to a flexible headcap worn by the subject. Because their positions are not fixed, Lorentz forces from B_0 and switching gradient fields can exert forces on the loops around the patient. Considering 2A with a range of loop sizes from 8cm diameter to 12cm diameter, the maximum Lorentz force observed will be under 0.4 grams, which doesn't expose any concerning safety risks.

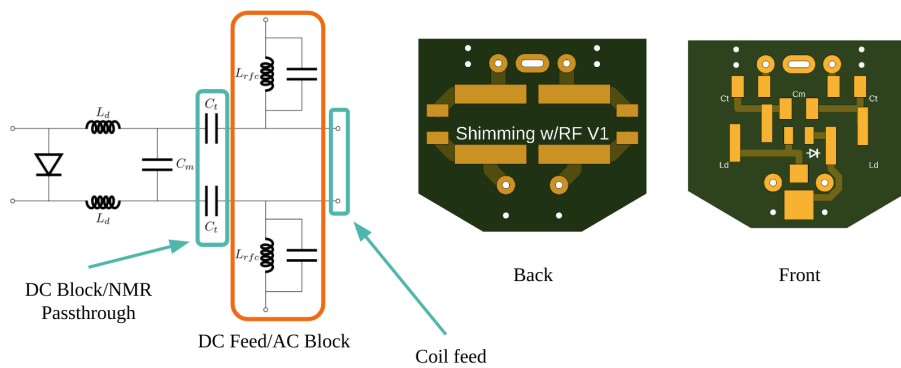


Figure 4.1: AC/DC Circuit. **Left** shows the circuit diagram of a typical RF receive coil. It features DC feed points which block the Larmor Frequency and AC feed points with DC blocks via capacitors. **Right**: initial PCB layout to allow for shim components on one side and RF components on the other.

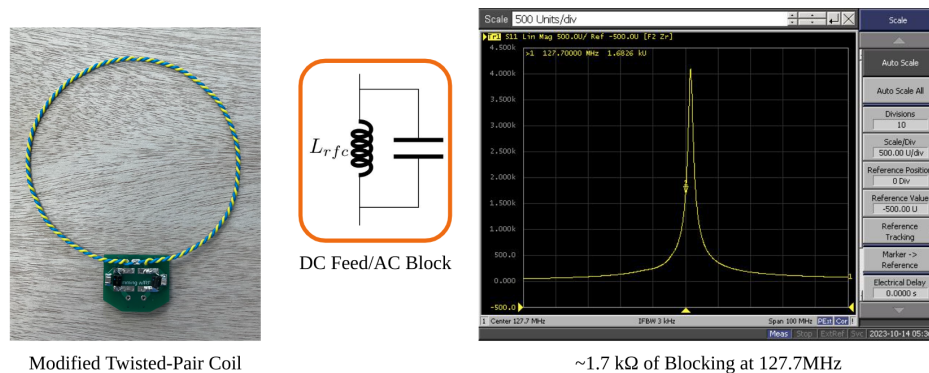


Figure 4.2: The blocking circuits implemented and tuned on one of the physical PCBs, showing sufficient impedance and blocking close to the Larmor Frequency.

Because the DC loops will be exposed to the strong RF pulses, it is imperative that the high impedance blocking circuits are added so that the current driver boards are not inundated with large induced AC currents[19][20]. These blocking circuits take the form of an LC circuit in parallel that is placed between the loop and the current driver. Because they are tuned to block the Larmor frequency for H_1 , they are often referred to as Proton traps. The excitation frequency is typically only emitted within a small bandwidth around the Larmor Frequency, thus the trap itself does not need to have a large blocking bandwidth. Figure 4.1 shows the DC feed and trap circuit added to a traditional Rx RF coil.

To tune the proton trap, one usually uses a double probe setup hooked up to a vector network analyzer with an S21 measurement. Though as shown by Shrestha et. al[18], using a single small sniffer loop to probe the *disconnected* proton trap is best for accurately distinguishing the response of the circuit. Adding the loop on the board will skew the measurement. Figure 4.2 shows a close up view of the board with a coil added to it and the VNA display used to tune the boards. Figure 4.3 explains the procedure used to tune and fix the proton traps so they can be tuned without upsetting the resonant frequency.

The loops themselves are not the only place where the excitation process could induce currents. The leads connecting the loops and the current drivers are also susceptible. As such, the leads to each loop are twisted to reduce noise, and also common mode traps are used to block common mode along the wires. These blocking circuits are not shown in the circuitry of the shim system; however, they wrap the leads and diminish common mode via coupling. Special Caterpillar Traps designed and built by Ekin Karasan[9] are used as shown in the V1 head array in Figure 4.4.

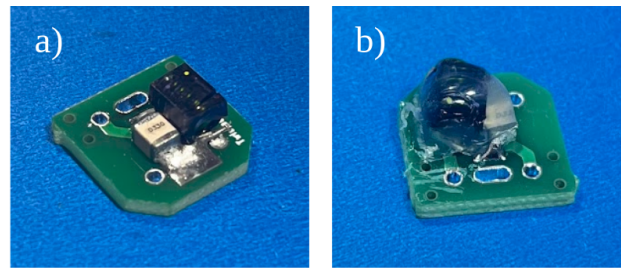


Figure 4.3: Tuning Process for proton traps. **a)** Shows the blocking LC circuit soldered onto a smaller V2 board. A 33 pF capacitor and a 47 nH inductor are used for the circuit. The inductor is then widened to increase the resonant frequency until the VNA display (seen in Figure 4.2) shows resonance at the Larmor Frequency, 127.7 MHz. **b)** Because the inductor is still malleable after tuning and handling it will likely de-tune the trap, it is covered in hot glue to hold its position.

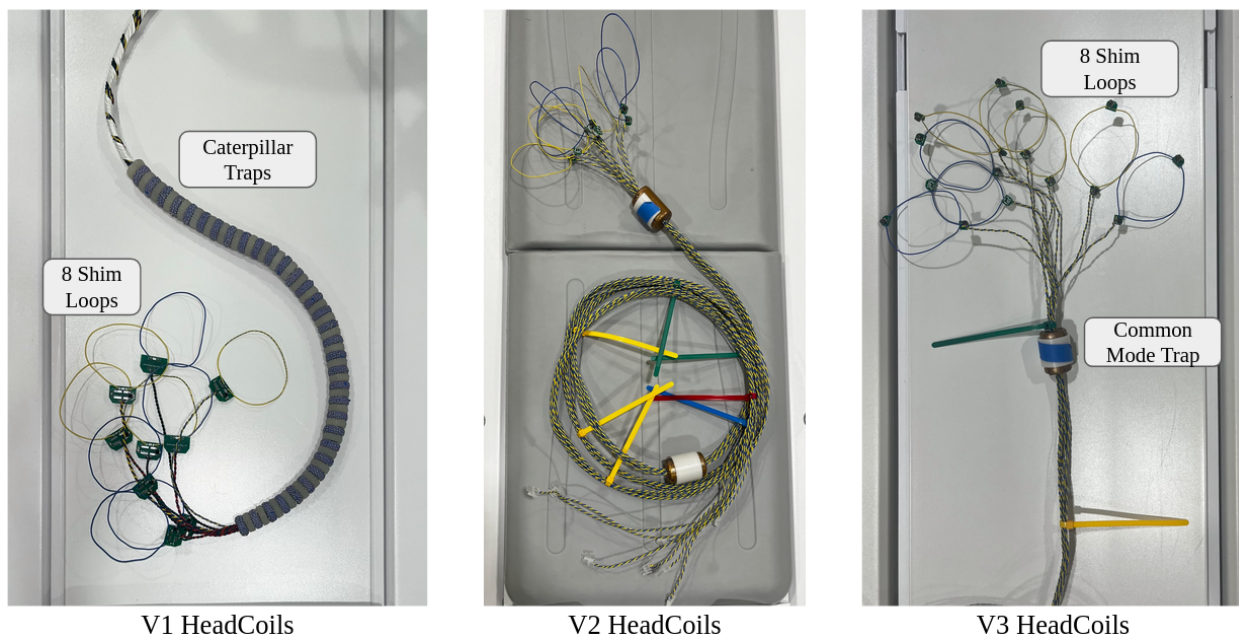


Figure 4.4: 8 shim loops constructed, each with its own lead going to the shim current driver. In V1, Caterpillar Traps are featured wrapping the wire to induce blocking of common mode currents along the leads themselves[9]. In V2, the boards containing the proton traps were minimized to reduce B1 artifacts caused by the wire traces on the boards. In V3, an extra blocking proton trap was added in-line to each of the shim loops to further reduce Larmor Frequency. V2 and V3 also feature individual baylun traps instead of the caterpillar traps.

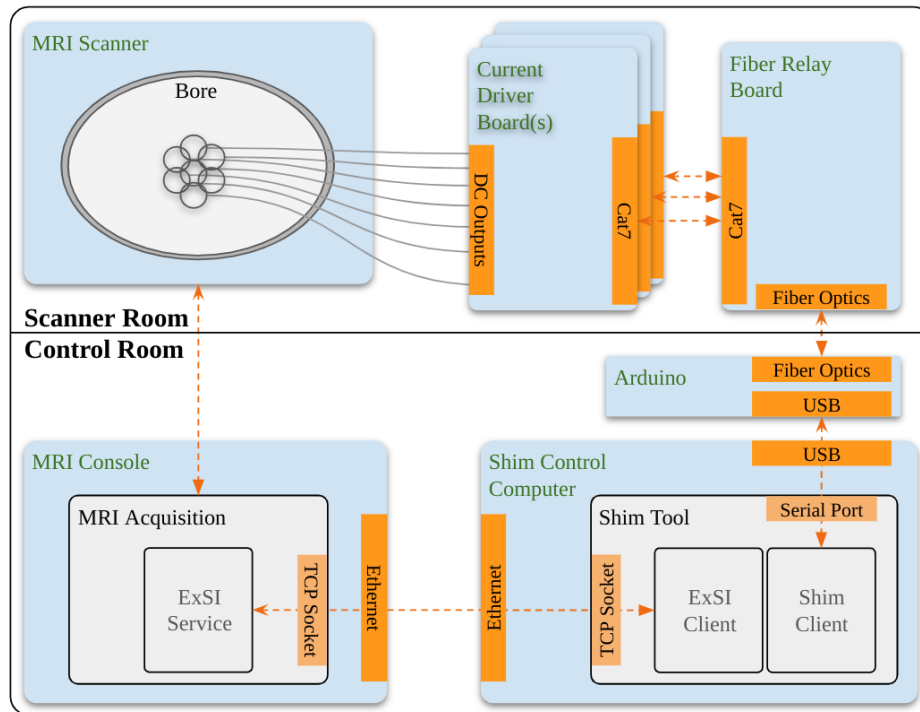


Figure 4.5: System Overview of the Shim Tool. The tool itself runs on a separate computer from the MRI Console for software availability and different scanner version compatibility. It features two client services that control direct connectivity with the ExSI Server on the MRI Console and the boards controlling the actual shim array in the scanner. The Shim tool synchronizes asynchronous operations between ExSI and the Shim Drivers, provides a user interface that describes current operations, and allows a user to begin a host of optimally shimmed scans with a defined ROI at their will.

4.2 Tool System Design

Scanner Control

The scanner is controlled via the ExSI Server-Client communication protocol defined by GE. TCP messages are sent over a predefined socket and can instruct the MRI scanner to perform almost any function that one could have it do manually. A non-exhaustive list of commands that you could send to the scanner:

- `ConnectToScanner`: Allows Client to establish ExSI connection.
- `NotifyEvent`: Enables the scanner to notify on all events such as scan complete, prescan complete. Used for timing and sequencing of asynchronous commands.

- `SelectTask`: Selects the task desired to be modified.
- `ActivateTask`: Downloads the current task prescription to the scanner so it's ready to scan.
- `Scan`: Begins the currently activated scan.
- `PatientTable`: Allows moving the patient table so FOV is at isocenter.
- `LoadProtocol`: Loads a desired protocol into the task list of the console machine.
- `SetCVs`: Allows setting of task specific control variables once the task is activated.
- `Prescan`: Allows the user to initiate prescan or skip it for the current task.
- `GetExamInfo`: Provides the exam number and patient name of the scan. Used to locate directory on the scanner computer where files are saved from the session.
- `GetPrescanValues`: Provides the center frequency and shims that are set during prescan.
- `SetGrxSlices`: Allows the user to define the location of the FOV in the current scan.
- `SetShimValues`: Allows the user to set linear gradient shim center positions.

A Python based ExSI Client was written in a multi-threaded fashion so that commands could be sent out-of-sync from when they are received by the Shim Tool to be executed. As such, the ExSI Client exposes a queue to which other threads could append commands that get executed as soon as the scanner is in a ready and idle state to do so. Additionally, the ExSI Client exposes control variables that signal across threads on when certain events occur such as: 'command executed' on server, 'images acquired' so that image retrieval could begin, 'ExSI Connection Established' so that the shim tool knows it could begin standard operation. Moreover, the ExSI Client is capable of sending the Shim Driver Client a command to set currents of the Shim Loops at the exact time that it begins a scan, such that proper timing and execution of sequences could be followed in the full shim procedure.

Shim Control

The Arduino from the OpenSource Imaging current driver system exposes a similar command execution environment over the serial USB connection. Initially, currents could only be set according to a pre-programmed list containing user-inputted currents for various triggers. However, this interface was modified to receive commands for directly setting current on a specific channel. Additionally, code was added for the shim driver to acknowledge whenever a command is successfully processed or failed. This allows external software to dynamically control the state of the current driver system. The list of commands that you can execute on the shim system includes:

- Calibrate: Calibrates channels to ensure that they are connected correctly with the current driver boards.
- Zero: Sets all currents on all channels to 0A.
- ListCurrents: Receives a message with all the currents flowing on all the channels as seen by the ADC on the current driver board.
- SetCurrent: Allows the user to define a channel and set the desired current up to 2A.

The Shim Client is a custom written Python program similar to the ExSI Client that handles communication with the Arduino out of band from the thread that interfaces with the scanner and shim calculations. It likewise exposes a queue to the Shim Tool Program upon which commands can be lined up to be executed once the shim Arduino replies that it is ready. It also exposes a similar control variable to notify once the connection to the shim system has been validated.

Interface

The Shim Tool orchestrates sequences of shimming operations between both the ExSI Client and Shim Client, while providing control and diagnostic information to a user via a graphical user interface on the Shim Control Computer. A detailed diagram of the entire system and how the connections are distributed between computers / boards is shown in Figure 4.5. Beyond allowing the user to manually set the shim currents for any connected channel, run independent exams, and view the reconstructed data in the same GUI immediately slice by slice, the Shim Tool allows the user to, from a single button click, obtain background B_0 maps, individual B_0 basis maps for every single loop, as well as the linear gradients, apply shims for the desired slice, and also obtain shimmed B_0 maps. In addition to being able to simply do these operations, the GUI displays the B_0 maps of the background, of the expected optimal results, and of the actual shimmed result immediately when they are computed. Statistics are shown from each type of rendition for every slice, including mean, standard deviation, and median. The user is also allowed to selectively define a region of interest using the magnitude image obtained after the background map is taken. Currently, this ROI resizing feature is capable of defining any positioned or stretched ellipsoid across the three-dimensional FOV. The Shim Tool provides a visualization function to show the highlighted ROI while being crafted by the user. In the future, it is directly possible to include more shapes and methods for repositioning and stretching the ROI or even hand drawing desired spaces.

Use Case and Optimizations

There were a host of optimizations performed to verify and also speed up acquisition of calibration data as fast as possible. The number of scans that need to be acquired per

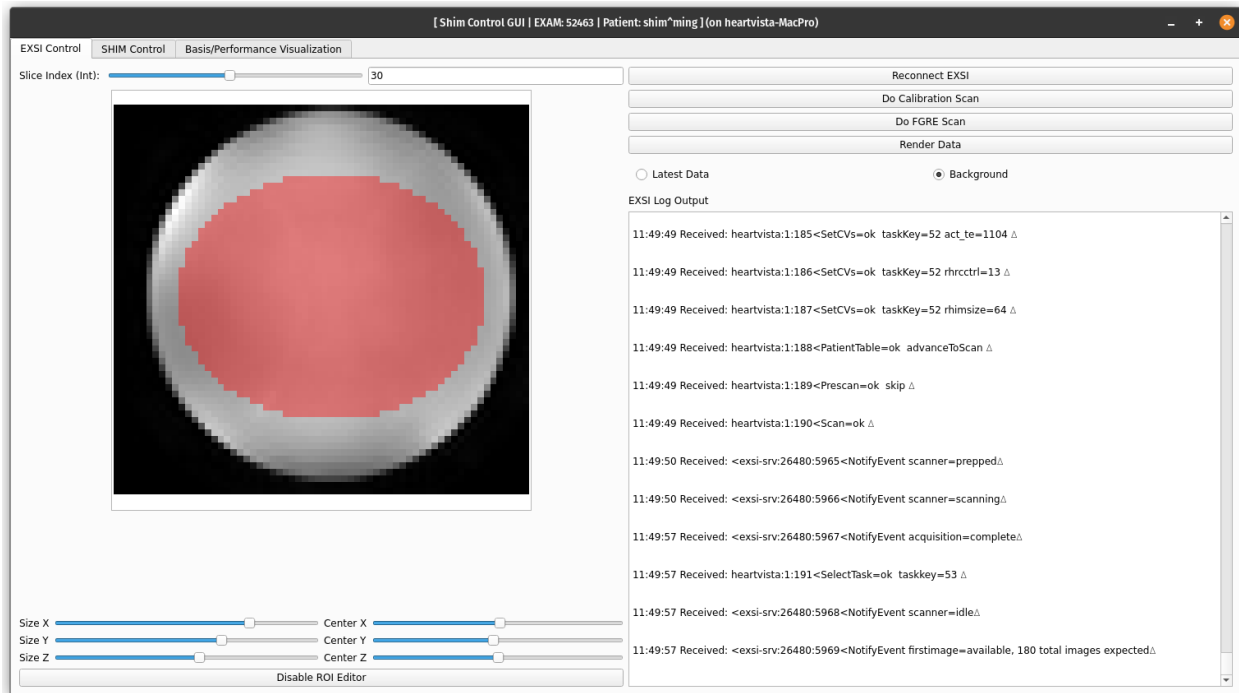


Figure 4.6: The Introductory view of the Shim Tool. Shows a log of ExSI Client-Server interaction, and allows the user to queue up predefined scan operations in addition to viewing axial slices one by one on the left. In addition to viewing the latest scan magnitude data, this view also allows the user to load the original magnitude image of the obtained background and define an ROI by overlaying an ellipsoid in transparent red. This ROI effectively truncates the data that is used to form basis vectors and the original background field. It is re-definable however many times the user wishes.

calibration sequence are on the order of the number of loops used. Multi-echo 3D GRE sequences were not of interest due to their lack of configurable TE's within less than a couple milliseconds of one another. While a short delta TE will increase the noise of B_0 map reconstruction, the problem of phase wrapping is simplified, and the field maps could be processed quicker. For simplicity, it was decided to use two separate Fast GRE sequences with different TEs set on them at a nominal 0.5ms Δ TE. This was optimal because the duration of the scans could be further shortened down to under 7 seconds each using parallel imaging and reconstruction ASSET, and many would be able to be quickly queued up sequentially using the new ExSI client. Lastly, a phase unwrapping algorithm was used within the SciKit-Image library, as introduced by Herraes [8], to unwrap accrued phase and make the tool robust to a variety of selected Δ TE selections.

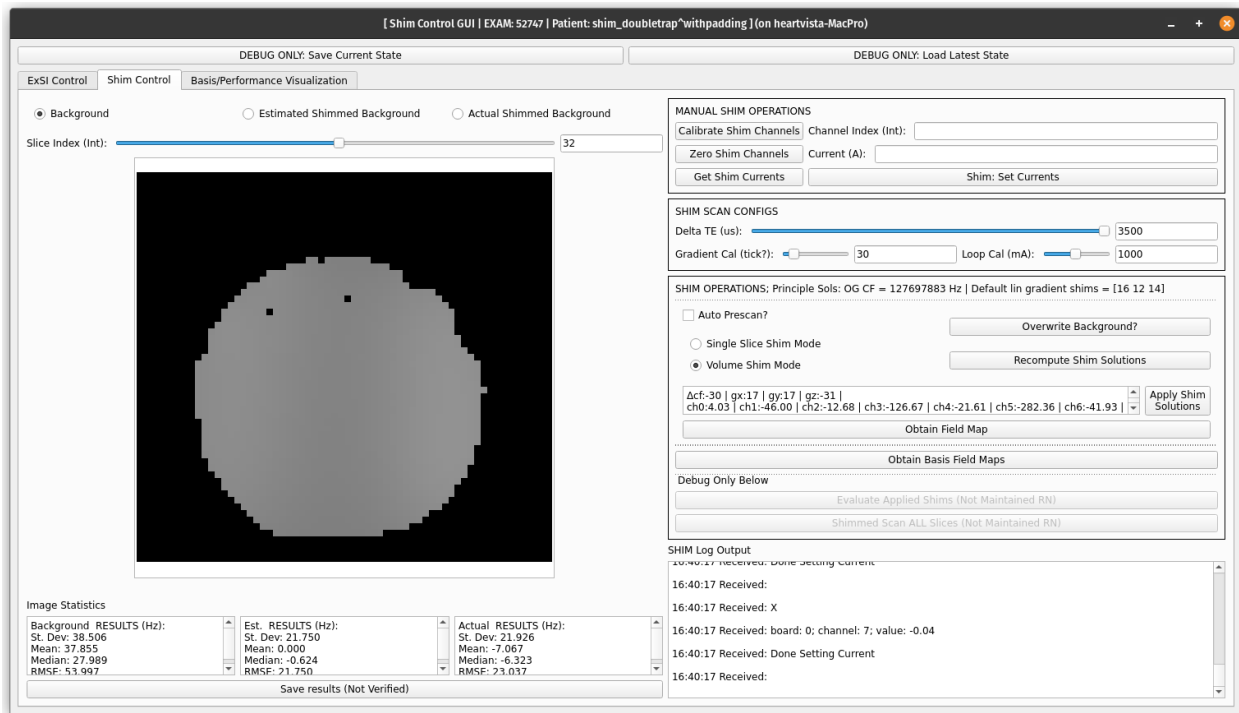


Figure 4.7: The Shim View of the Shim Tool. Shows log of communication with the Shim Drivers. It allows you to manually set currents to the shim loops, control the currently viewed slice index, set the delta TE between scans of phase images, obtain background or shimmed fieldmaps, loop and gradient basis maps. The left panes allow the user to switch between viewing the selected slice for either the background, the expected potential shim result, and the actual shim result of the scanned object. The bottom left allows the user to see statistics on each image and also save both data and statistics of performance of the shims once they have been acquired.

Chapter 5

Experimentation and Results

In practice, the Shim Tool removes the need for any human intervention with the scanner during shim calibrations. This is convenient considering calibration of *conformal* shim loops requires that new basis functions be acquired every time they are in a new position, or realistically every time a new subject uses them. The basis function of a shim loop consists of the fieldmap solely generated by that loop running 1A. Every B_0 fieldmap is constructed from two fast gradient echo (FGRE) scans as shown by Equation 2.5. Thus, the total time for calibrating N shim loops is the sum of: the time it takes to do one prescan, time to do one background fieldmap, and time to acquire a B_0 map for every loop with a calibration current; there also needs to be a basis map acquired for linear gradients unless they are pre-recorded / modeled. This gives $(N + 1) \times T_{2\text{FGRE}} + T_{\text{Prescan}}$ as the total time for the scan. The GRE sequence used has a FOV of 19.2 cm by 19.2cm by 18cm, with 3mm isometric voxels, TE of between 1.1ms and 4.1ms, and 64 phase and frequency encodes in order to optimize for scan duration. Experimentally, it was found that a prescan takes about 30 seconds, and each scan takes between 23-30 seconds. There are also non-deterministic delays when the scanner *Activates* a task or *Loads New Protocol*. For 8 loops, and a ΔTE of 3.5 ms for the B_0 maps, it takes a little under 10 minutes to complete calibration in this manner.

To characterize the performance of the shim loops, a sphere phantom is equipped with the 8 loop shim array, and the quality of reconstructed images is compared before and after shimming. To effectively stress the system and show it correcting reasonable artifacts, water bottles and a TMS Coil were used to induce off-resonance. An axial slice is imaged close to the shim loops using the Balanced Steady State Free Precession (bSSFP) and Gradient Echo Planar Imaging (EPI) protocols, which are both sensitive to off-resonance artifacts. Scan parameters for each of the images are included in the descriptions of Figures 5.5 and 5.6. Figure 5.1 shows the phantom setup used in the scanner and how the shim loops are patterned around it. Figure 5.2 displays the specific setups of the three experiments performed. Figure 5.3 shows the B_0 fieldmaps, with statistics, before and after shimming for each experiment. Figure 5.4 shows performance of the shim tool and hardware as a histogram for the slice that is shimmed in each experiment. Figure 5.5 and 5.6 show bSSFP and EPI images acquired before and after shimming.

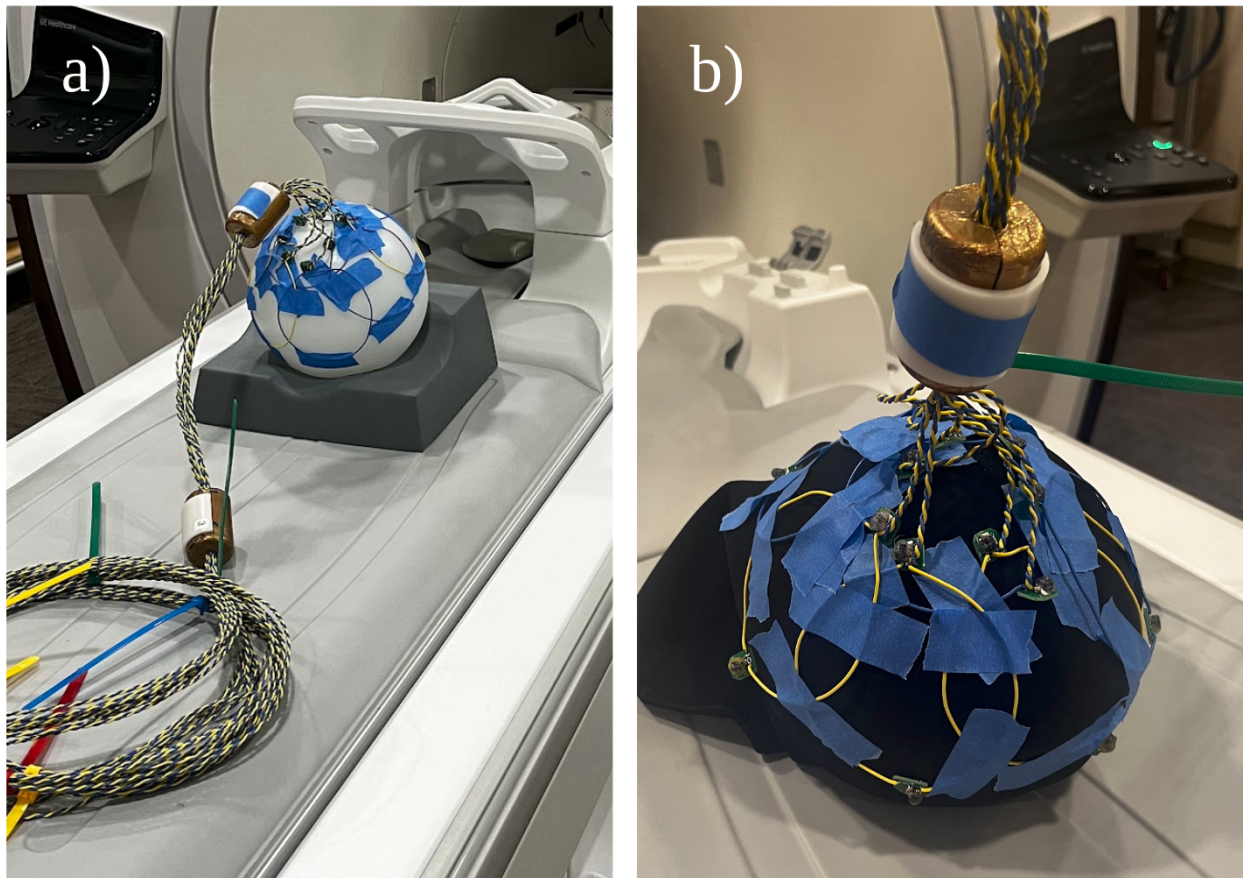


Figure 5.1: Setup of Phantom and shim loops. **a)** The sphere phantom with 8 shim loops taped around the phantom. They are arranged with one loop in an axial position in the center and 7 loops around it. **b)** The same sphere phantom is covered by a 3mm thick head mask with shim elements taped around it in the same orientation as in (a). A head mask with stitched on AC/DC elements will eventually facilitate a simple method for equipping the coils to the subject.

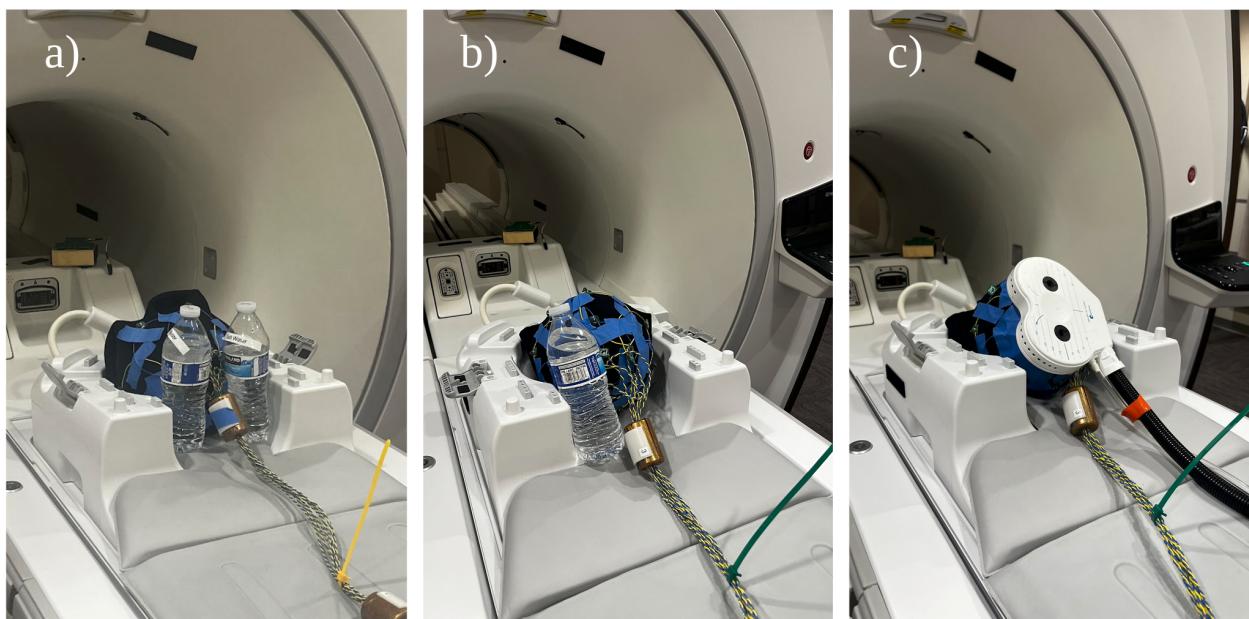


Figure 5.2: Experimental setups to induce off-resonance. **a)** The shim-loop-equipped phantom with two water bottles to induce B_0 off-resonance. **b)** With one water bottle. **c)** With a TMS Coil. The off-resonance from a TMS Coil, and the robot arm around it, is largely the motivation for this project.

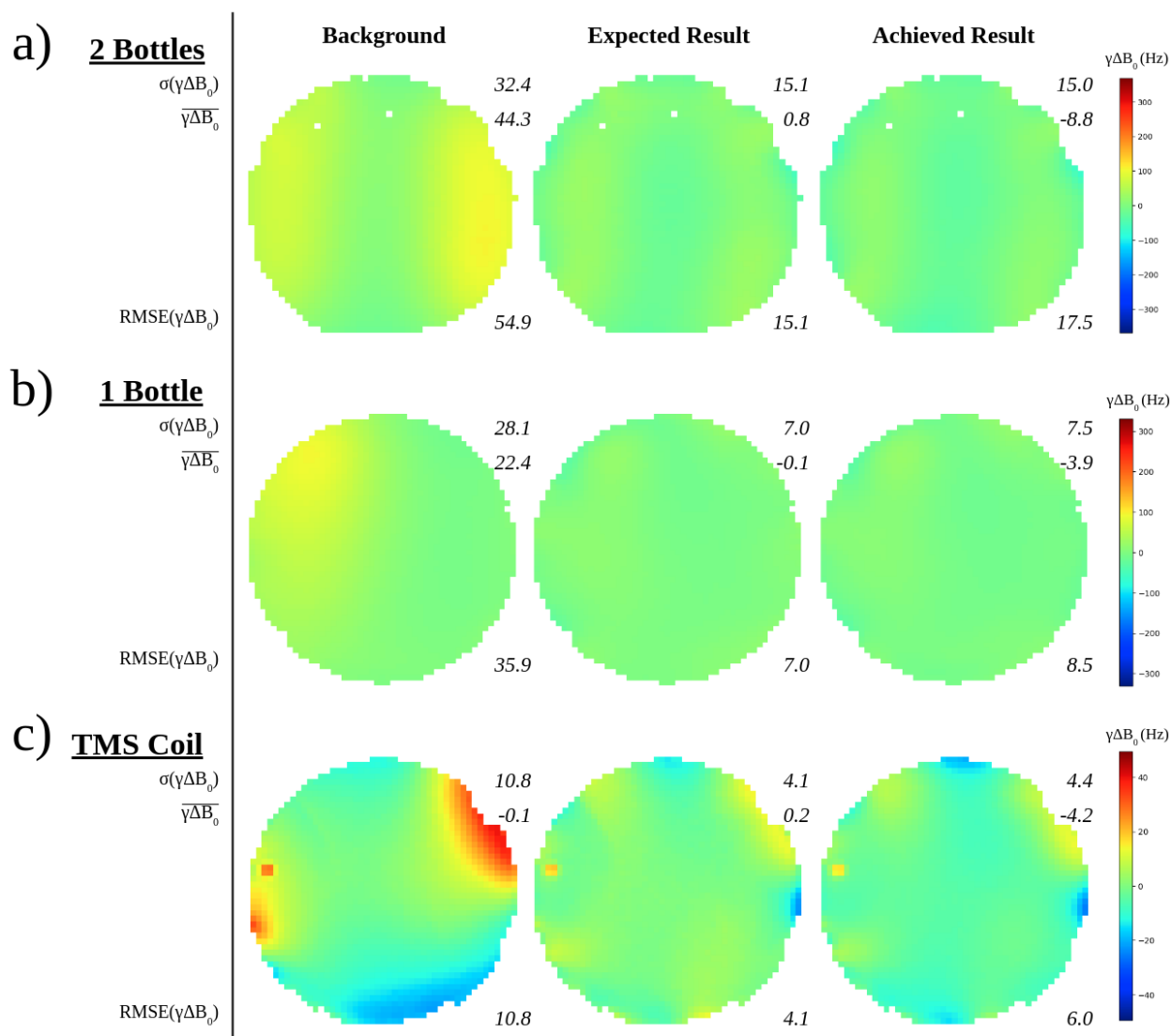


Figure 5.3: Shim performance, as observed by the Shimming Tool, in terms of visualized B_0 maps for each experiment. The Background, Expected, and Achieved B_0 fieldmaps are shown for all three experiments. The Background is the fieldmap without any shimming done. The Expected is the fieldmap that the shim tool computes that it should achieve. The Achieved is the fieldmap observed after shimming. Note: the color scales of the 2 Bottle and 1 Bottle experiments are on the order of 300 Hz, while the TMS coil experiment is on the order of 40 Hz. The standard deviation and mean of off-resonance in the slice is shown in terms of Hz for each fieldmap. The Shim Tool and hardware reduce overall root mean squared error by 63 percent on average.

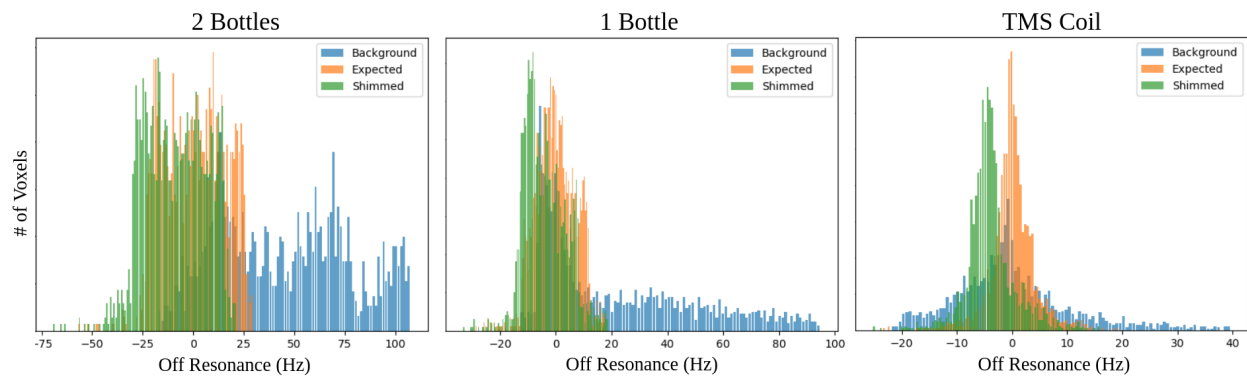
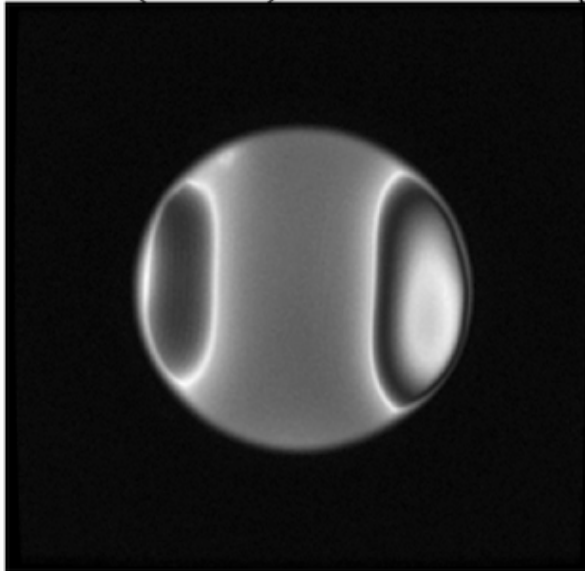


Figure 5.4: Histogram showing voxels binned by the amount of off-resonance they have for each experiment. In each histogram, the Background, Expected, and Shimmed corrected fieldmaps are shown in different colors. The Background is the fieldmap without any shimming done. The Expected is the fieldmap that the shim tool computes that it should achieve. The Shimmed is the fieldmap observed after shimming.

2 Bottles: bSSFP and 4 Shot EPI

Fiesta (bSSFP) Before Shimming



Fiesta (bSSFP) After Shimming

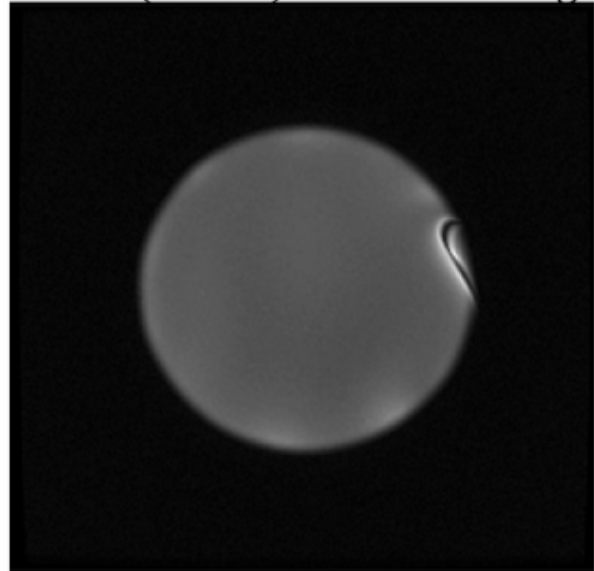


Figure 5.5: 2 Bottle Experiment: bSSFP images before and after shimming. They were acquired with a 24 by 24 cm FOV in the same position that the shim tool was correcting and 256 frequency and phase encodes. The bSSFP scan has a TE of 2.3 ms and TR of 6.7 ms

1 Bottle: bSSFP and Single Shot GRE EPI

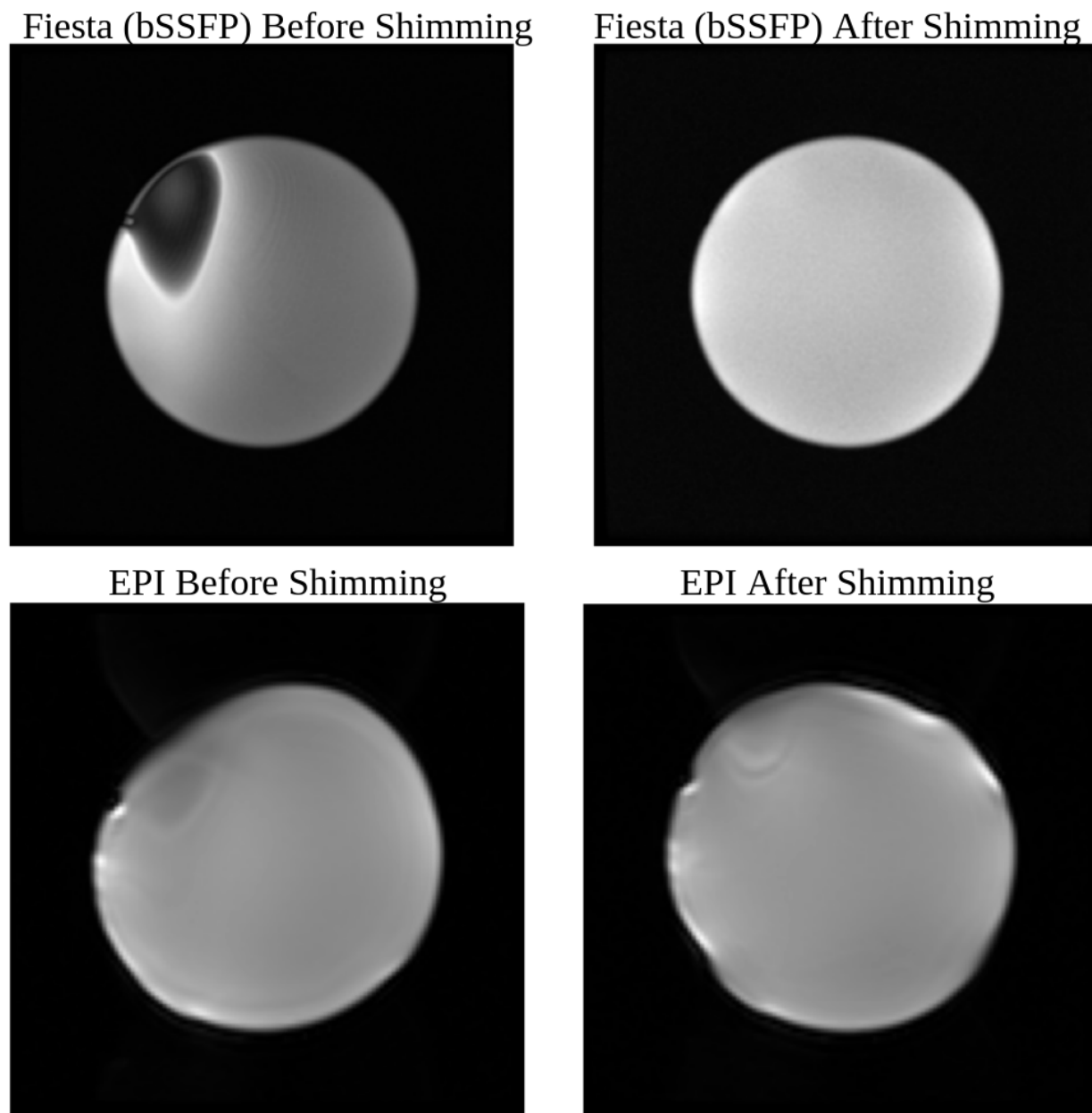


Figure 5.6: 1 Bottle Experiment: bSSFP and single shot EPI images before and after shimming. They were acquired in the same position that the shim tool was correcting. The bSSFP scan has a TE of 2.1 ms, TR of 6.3 ms, 24 by 24 cm FOV, with 224 frequency and phase encodes. The EPI scan has a TE of 20.1 ms and TR of 149 ms, 22 by 22 cm FOV, with 96 frequency and phase encodes.

Chapter 6

Discussion

6.1 Conclusion

This project presented an adaptable automated shimming tool and conformal local B_0 shim array. While it was implemented on the GE MR750 3T scanner, it can be used with any MRI system. The B_0 shim array was fabricated by hand using MR safe materials, and boards were fabricated to block AC currents while scanning. The Shim Tool automated control of the scanner for numerous scans and made the tedious process of calibrating every shim loop quicker. Furthermore, the ExSI client developed for the Shim Tool is a ubiquitous asset to the GE scanner and enables users to automate any lengthy scan procedure using a custom Python script or Jupyter Notebook.

Through experimentation, the Shim Tool effectively reduced B_0 inhomogeneity and resulted in clearer scans with less signal loss for scans sensitive to field fluctuations. The setup with 8 shim loops allowed root mean squared error (RMSE) of field inhomogeneity (averaged between the 2 Bottle, 1 Bottle, and TMS Coil experiments) to decrease by 63 percent. The tool is adaptable to any number of shim coils provided that the Open Source Imaging Current Drivers can support them and that the shim loops are equipped with well tuned proton traps.

6.2 Future Work

AC/DC Coil Integration

Beyond further developing the shim boards with better tuned proton traps, integration with Rx/Tx coils is immediately necessary. This poses significant non-trivial work as the shim path needs to be isolated from any AC and needs to not degrade any of the functionality of the Rx/Tx performance.

Shim Tool Feature Improvement

There are a host of feature improvements to be integrated into the Shim Tool as it gains use and matures, such as:

- More ROI shapes including custom draw-able ones and brain extraction with FTE.
- Integration with the scanner system, along with cabling routed through the scanner bed.
- Customized pulse sequences and triggers to initiate shim settings with.
- Likely a UI revamp to pack the extra features more accessibly.
- Many more future items are illustrated on the Github Issues page for the project.

There will also be more work to speed up the time it takes to acquire basis maps of the conformal shim array. Using incredibly fast, and serialized sequences such as VNaves or custom sequences / scanner code that would signal when to change calibration currents will be necessary if this system is ever to be used in a clinical setting.

Bibliography

- [1] Suma Anand and Michael Lustig. *Beat Pilot Tone (BPT): Simultaneous MR Imaging and RF Motion Sensing at Arbitrary Frequencies*. 2024. arXiv: 2306.10236 [physics.med-ph]. URL: <https://arxiv.org/abs/2306.10236>.
- [2] Nick Arango et al. “Open-source, low-cost, flexible, current feedback-controlled driver circuit for local B0 shim coils and other applications”. In: *Int Soc Magn Res Med*. Vol. 1157. 2016, p. 6.
- [3] Andreas Bungert et al. “Reducing image artefacts in concurrent TMS/fMRI by passive shimming”. In: *NeuroImage* 59.3 (2012), pp. 2167–2174. ISSN: 1053-8119. DOI: <https://doi.org/10.1016/j.neuroimage.2011.10.013>. URL: <https://www.sciencedirect.com/science/article/pii/S1053811911011748>.
- [4] Rafael Calleja and Celine Veys. “Local B0 Shim Array Integrated onto a Solenoid TRX Coil for Permanent Magnet Scanners”. In: (2021).
- [5] Jonathan David Cuthbertson. “The iPRES-W Coil: An MRI RF Coil for Simultaneous MR Image Acquisition, Wireless Communication, and Localized B0 Shimming”. In: (2018).
- [6] Douglas C. Giancoli. *Physics for Scientists and Engineers*. Englewood Cliffs, N.J.: Prentice Hall, 1989.
- [7] Jordan Grelling. “An Automated Control System for Beat Pilot Tone in MRI”. In: (2022).
- [8] Miguel Arevallilo Herráez et al. “Fast two-dimensional phase-unwrapping algorithm based on sorting by reliability following a noncontinuous path”. In: *Appl. Opt.* (2002).
- [9] Ekin Karasan et al. “Caterpillar traps: A highly flexible, distributed system of toroidal cable traps”. In: *Magnetic Resonance in Medicine* 89.6 (2023), pp. 2471–2484.
- [10] Feng Liu et al. “A Hybrid Field-Harmonics Approach for Passive Shimming Design in MRI”. In: *IEEE Transactions on Applied Superconductivity* 21.2 (2011), pp. 60–67. DOI: 10.1109/TASC.2011.2112358. URL: <https://ieeexplore.ieee.org/stamp/stamp.jsp?tp=&arnumber=5724291>.
- [11] Julian Adolfo Maravilla. “15-channel head cap array using twisted pair elements for MRI.” In: *Proc. ISMRM*. Vol. 31. 2023.

- [12] et al. Navarro de Lara. “A wearable “RF-EEG Cap” for full head coverage concurrent TMS/EEG/fMRI experiments at 3T: a feasibility study”. In: *Proc. IMRM*. 2021.
- [13] Dwight Nishimura. *Magnetic resonance imaging: physical principles and applications*. Elsevier, 2000.
- [14] John Pauly. “Field Maps”. 2005. URL: <https://ece-classes.usc.edu/ee591/library/Pauly-FieldMaps.pdf>.
- [15] Judith C. Peters et al. “On the feasibility of concurrent human TMS-EEG-fMRI measurements”. In: *Journal of Neurophysiology* 109.4 (2013). PMID: 23221407, pp. 1214–1227. DOI: 10.1152/jn.00071.2012. URL: <https://doi.org/10.1152/jn.00071.2012>.
- [16] Justin Riddle et al. “A guide for concurrent TMS-fMRI to investigate functional brain networks”. In: *Frontiers in Human Neuroscience* 16 (2022). ISSN: 1662-5161. DOI: 10.3389/fnhum.2022.1050605. URL: <https://www.frontiersin.org/articles/10.3389/fnhum.2022.1050605>.
- [17] John F. Schenck. “The role of magnetic susceptibility in magnetic resonance imaging: MRI magnetic compatibility of the first and second kinds”. In: *Medical Physics* 23.6 (1996), pp. 815–850. DOI: <https://doi.org/10.1118/1.597854>.
- [18] Manisha Shrestha et al. “Considerations for Accurate Active Detuning Measurements in Densely Parallel Array Coils”. In: *ISMRM*. 2023. URL: <https://cds.ismrm.org/protected/23MPresentations/abstracts/3911.html>.
- [19] Jason P. Stockmann and et al. “A 31-channel integrated “AC/DC” B0 shim and radiofrequency receive array coil for improved 7T MRI”. In: *Magnetic Resonance in Medicine* 87.2 (2022), pp. 1074–1092.
- [20] Trong-Kha Truong, Dean Darnell, and Allen W. Song. “Integrated RF/shim coil array for parallel reception and localized B0 shimming in the human brain”. In: *NeuroImage* 103 (2014), pp. 235–240. ISSN: 1053-8119. DOI: <https://doi.org/10.1016/j.neuroimage.2014.09.052>. URL: <https://www.sciencedirect.com/science/article/pii/S1053811914007940>.
- [21] Celine Veys and Rafael Calleja. “Integrating a Localized B0 Shim Array into a Solenoid Transmit-Receive Coil for Permanent Magnet Scanners”. In: (2021).

Appendix A

Code

The code is available at: https://github.com/mikgroup/ge3t_shim_tool